

A precision test of the isotropy of the speed of light using rotating cryogenic optical cavities

S. Schiller, P. Antonini, and M. Okhapkin

Institut für Experimentalphysik, Heinrich-Heine-Universität Düsseldorf,
40225 Düsseldorf, Germany.

Summary. A test of Lorentz invariance for electromagnetic waves was performed by comparing the resonance frequencies of two stable optical resonators as a function of orientation in space. The crystalline resonators were operated at 3.4 K in a cryostat employing a pulse-tube refrigerator. A new analysis yields the Robertson-Mansouri-Sexl theory parameter combination $\beta - \delta - 1/2 = (-0.6 \pm 2.1 \pm 1.2) \cdot 10^{-10}$ and one parameter of the Standard Model Extension theory, $(\tilde{\kappa}_{e-})^{ZZ} = (-2.9 \pm 2.2) \cdot 10^{-14}$.

1.1 Introduction

The isotropy of space is a well-tested symmetry of nature [1]. Because it is a foundation of today's accepted theories of the fundamental forces it continues to be the focus of both theoretical and experimental studies. A series of experiments [2, 3, 4] have recently been performed with the goal of improving the limits for a hypothetical violation. They were in part motivated by the development of an extension of the Standard Model (SME) by Kostelecký and coworkers [5, 6] that describes Lorentz violation in a comprehensive way. This dynamical test theory indicates that isotropy violation, if it exists, may exhibit characteristics that differ from those of previous kinematic test theories, such as the Robertson-Mansouri-Sexl (RMS) theory [7].

Here, we will not discuss the conceptual frameworks used to describe hypothetical violations of isotropy, since this is reported in the literature and is also treated in this Proceedings volume. In this contribution, we limit ourselves to the description of an experiment used to perform an improved test of the isotropy of the speed of light. The experiment has already been presented previously [8]; here we give a more detailed description and report an extension of the data analysis.

The experiment was conceived as an actively rotated Michelson-Morley experiment using ultrastable optical cavities interrogated by lasers. It was a natural extension of our previous work with stationary resonators [3, 9], but employed a completely new apparatus, except for the sapphire optical cavities.

The experiment consists in measuring the difference (beat) $\nu_1 - \nu_2$ between the frequencies of two longitudinal modes of two orthogonal standing-wave cavities as a function of orientation in space. If isotropy is violated, according to the Robertson-Mansouri-Sexl test theory and the Standard Model extension, the beat frequency will vary as

$$\frac{\delta(\nu_1(t) - \nu_2(t))}{\nu} = 2B(t) \sin 2\theta(t) + 2C(t) \cos 2\theta(t), \quad (1.1)$$

where $\nu_1 \approx \nu_2 \approx \nu$ is the average frequency ($2.8 \cdot 10^{14}$ Hz in this experiment) and $\theta(t)$ is the angle between one cavity's axis relative to the south direction.

In the RMS test theory, the amplitudes $2B(t)$ and $2C(t)$ are proportional to the parameter combination $\beta - \delta - 1/2$, where β , δ parametrize deviations of the frame transformation equations from the usual Lorentz form. The explicit form is given below.

In the SME test theory [5], each amplitude $2B(t)$ and $2C(t)$ is a linear combination of eight coefficients weighted by time-harmonic factors. The amplitude $B(t)$ contains frequency components at 0 , ω_{\oplus} , $2\omega_{\oplus}$, $\omega_{\oplus} \pm \Omega_{\oplus}$ and $2\omega_{\oplus} \pm \Omega_{\oplus}$, while $C(t)$ contains in addition one component at the frequency Ω_{\oplus} . Here ω_{\oplus} is Earth's sidereal angular frequency and Ω_{\oplus} is Earth's orbital frequency. The determination of the individual $\tilde{\kappa}_{o+}$ coefficients requires the ability to resolve the contribution of Earth's orbital motion in order to discriminate between modulation frequencies differing by Ω_{\oplus} . Thus a measurement extending over at least 1 year is necessary. However, in this experiment we concentrated on a single parameter, $(\tilde{\kappa}_{e-})^{ZZ}$, and using previous results for the remaining parameters, it was possible to obtain a result within a much shorter measurement time.

1.2 Experimental setup

An overall view of the experimental setup is shown in Fig. 1.1. The whole setup was actively rotated by a computer-controlled precision ball bearing turntable. The turntable itself rested on an optical table ($3 \text{ m} \times 1.5 \text{ m}$) that was not floated. An octagonal base plate mounted on the turntable carried most of the components, except for the vacuum forepump, the Helium compressor, and a synthesizer. The cryostat was attached via columns to a plate that could be rested on top of a rack mounted on the base plate. Cryostat and plate could be removed from the rack for opening. On the plate the rotary valve and its driver, temperature controllers, dataloggers, synthesizers and power supplies were installed. The servo systems for the cavity frequency locks and the laser power stabilizations were mounted on the sides of the rack. The laser systems, enclosed by boxes, were located on a breadboard placed on the octagonal base plate. The beat frequency detector was contained in one of the boxes. Thermal insulation (not shown in the figure) was used to shield several of the components of the setup.

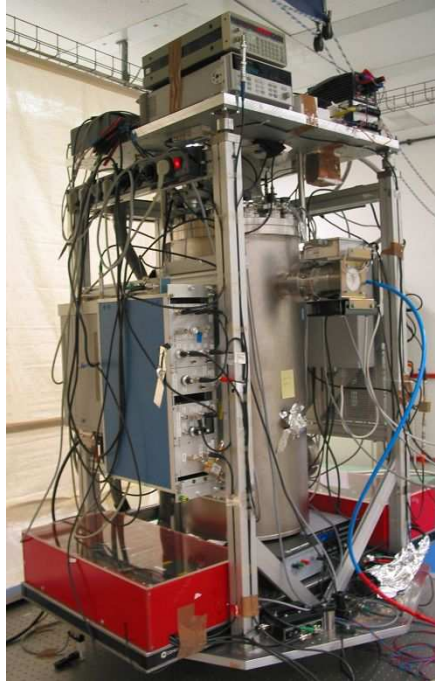


Fig. 1.1. The experimental setup. The turntable is located under the octagonal base plate and is not visible in the photograph. See text for details.

1.2.1 The cryogenics

The cryostat is sketched in Fig. 1.2. Cooling was implemented by a two-stage pulse-tube cooler [10] (Transmit GmbH), using high pressure (18 bar) Helium as working medium. The first stage had a high cooling power (6 W at 50 K) and reached a temperature of approx. 41 K, while the second had a lower cooling power (approx. 0.2 W at 3 K) but was able to reach a minimum temperature of about 2.2 K without load, and 3.2 K when loaded with the experimental set-up used for this experiment. The cooler was driven by a water-cooled Helium compressor (Leybold) with 6 kW power consumption. A significant advantage of this novel cooler type compared to standard cryocoolers is the absence of moving parts inside the cryostat; only the He gas moves within the cryostat, under periodically modulated pressure. Mechanical motion was, however, present in the rotary valve on the top plate. As a consequence, the displacement of the resonators was modulated at the rotary valve frequency, with an amplitude of approx. $1 \mu\text{m}$ vertically and horizontally, as determined from the propagation of the laser beam exiting the cavities.

An optical cryostat was used, containing three free-space optical access ports: two half-inch diameter windows for horizontal access and an additional window located at the bottom (not used here). Anti-reflection-coated BK7

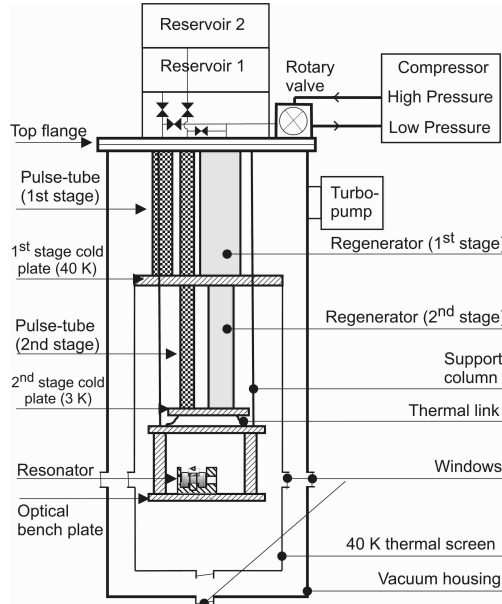


Fig. 1.2. Cut-away schematic of the cryostat with internal components (not to scale). Height and diameter of the vacuum housing are 90 and 40 cm, respectively. Only one resonator is shown.

was used as window material. To avoid backreflections, the windows' normals are angled with respect to the beam direction. The lateral ports were used during the laser alignment and frequency lock phases to identify the cavity modes excited by the lasers.

A copper heat shield (thermal screen) was attached to the first stage cold plate. To improve shielding from the 300 K vacuum can, it also contained angled windows. The space available below the second stage cold plate was about 30 cm in height and 30 cm in diameter. The experimental assembly consisted of an upper plate, four columns, and a bottom optical bench plate, all made of copper, rigidly connected together. It was attached to the top flange by 3 hollow stainless steel rods of 40 cm length, which were heat sunk to the first stage cold plate but not to the second stage cold plate [11]. Copper mesh provided the thermal link between the experimental assembly and the second stage cold plate. The assembly was thermally shielded by superinsulation foils.

A turbo pump was used to continuously evacuate the chamber. The top flange of the cryostat contained twelve KF flanges that were used for electrical signal and optical fiber vacuum feedthroughs.

After evacuation of the cryostat, the cool-down time to 3.2 K was about 12 hours.

On a timescale of 10 min, the temperature of the first stage varied by less than 0.1 K. On the optical bench plate, where the cavities are located, the

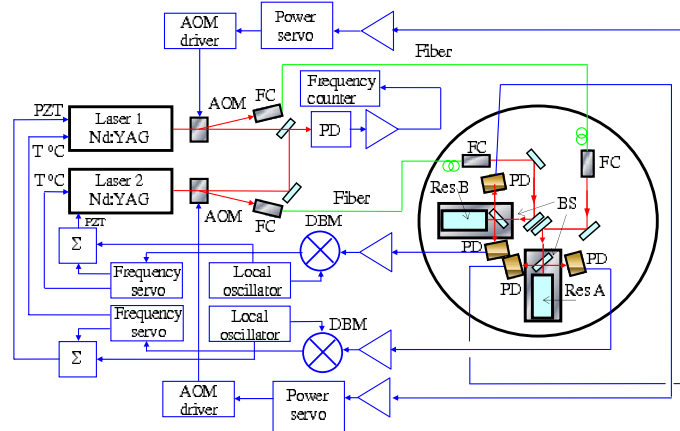


Fig. 1.3. Schematic of the opto-electronic system. Two Nd:YAG lasers (1064 nm) are frequency-locked to two sapphire optical resonators located in the cryostat. The beams are fed to the resonators via optical fibers. Acousto-optic modulators (AOM), stabilize the power of the beams fed to the resonators. DBM: doubly-balanced mixer; BS: beam splitter; PD: photodiode; FC: fiber coupler, PZT: piezoelectric frequency control actuator; T: temperature control of the laser crystal.

variations were significantly lower, with a 4 mK short-time (10 s) temperature instability and 50 mK instability over long times (10 h). These variations came from (small) instabilities of the pulse-tube cooler itself, and from a dependence of the temperature of the cold stages on the ambient temperature. To reduce these variations, the temperature of the resonators was kept stable at a value slightly above the second stage temperature by active temperature control. A combination of a heater attached to the underside of the optical bench plate, equidistant from the two optical resonators, and a high sensitivity thin film sensor fixed to one resonator housing, together with a commercial digital temperature controller was used, and kept the temperature constant at 3.4 K.

1.2.2 The optics setup

An overview of the functional parts of the laser and resonator system is shown in Fig. 1.3, and the components on the optics base plate are shown in Fig. 1.4.

The two optical resonators are made of pure sapphire (Al_2O_3) [12]. Each consists of a 3 cm long cylindrical spacer with inner diameter 1.0 cm, outer diameter 2.6 cm, and crystal c-axis parallel to the cylinder axis. The sapphire mirrors have 1 m radius of curvature and are optically contacted to the spacer. A small hole perpendicular to the cavity axis serves for evacuation. The mirrors are coated for high reflection at 1064 nm. These resonators were already used for relativity tests [3, 9, 13, 14]. The linewidths of the two resonators were 100 kHz at the time of the experiment.

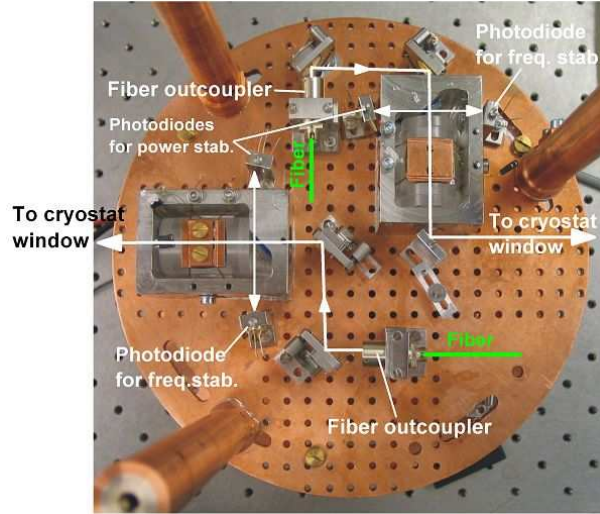


Fig. 1.4. View of the main cryogenic optical components located on the optics bench plate, without electrical cables and optical fibers. The resonator housings shown were later replaced by gold-plated copper housings.

Sapphire was chosen because of its very low thermal expansion coefficient at cryogenic temperature and its low dimensional drift [13]. For dielectric crystals, the thermal expansion is due solely to phonons and therefore the expansion coefficient drops as T^3 as the temperature T approaches zero. For sapphire the value at 3.4 K is approx. $8 \cdot 10^{-11} \text{ K}^{-1}$ [15]. We note, however, that the effective expansion coefficient of a mounted cavity can differ substantially, because it also involves the interaction of the resonator with its holder. Thus, in past experiments we have found zero crossings of the thermal expansion coefficient at 3 K [16].

In the present setup, the two resonators were mounted in two housings made of invar and coated with a $5 \mu\text{m}$ thick gold layer. Gold was used to obtain good contact between the resonators and their housings. The resonators were then fixed to the housing using thin copper straps. The straps were not strongly tightened, to avoid squeezing the resonators because of contraction of the straps during cool-down.

The laser beams were transported to the cavities via two 4 m long polarization-maintaining single-mode fibers with 8° angled fiber ends (to avoid back reflections and minimize etalon effects). The fiber ends were connected to fiber couplers containing short focal length lenses and rigidly attached to the optical base plate. For each laser beam, two adjustable vacuum compatible stainless steel mirror mounts deflected the light toward a 90% reflection/10% transmission beam splitter placed just before the cavity. The light directly reflected from the beam splitter reached a 2 mm diameter InGaAs photodiode that pro-

vided the signal for power monitoring and stabilization. The transmitted light was reflected by the cavity, then partially by the beam splitter and was sent to another photodetector of the same type to provide the signal for frequency locking.

The alignment of the laser beams was done at room temperature with the cryostat open. After cooling, the lasers were locked to the TEM₀₀ modes, which could be identified with the help of CCD cameras that monitored the cavity light leaving the cryostat through the windows. The coupling efficiency was typically 10% at room temperature. The efficiency was reduced by a factor 2 in the cold state due to differential thermal contraction effects.

Two diode-pumped monolithic non-planar ring oscillator Nd:YAG lasers emitting 200 mW at 1064 nm were used. The power fed into the fibers was about 1.5 mW. The Drever-Hall reflection locking scheme was used [17]. The lasers were phase modulated at frequencies of 300 kHz via the piezoelectric actuators acting on the laser crystals [18]. The error signals had typical SNR > 10 in a bandwidth of 100 kHz after amplification. They were processed by respective analog servos, each employing a loop for the laser piezoelectric actuator (unity gain coefficient at about 15 kHz) and a slow loop for laser crystal temperature control. The accuracy of the servo electronics was better than 0.1 Hz at 100 s integration time.

The power of each laser beam incident on the cavities was about 50 to 100 μ W and was actively stabilized to a relative level of $1 \cdot 10^{-4}$ using an acousto-optical modulator (AOM) placed before the fiber outside the cryostat. The AOMs also served as optical isolators.

On the laser breadboard, two parts of the laser beams were superimposed on a fast photodiode, producing a heterodyne signal at the beat frequency $\nu_1 - \nu_2$, about 700 MHz. This frequency was mixed down with a synthesizer to a frequency of about 10 MHz, to exploit the higher accuracy of the counter at lower frequencies. Both synthesizer and frequency counter were phase-locked to the 5 MHz output of a hydrogen maser.

1.3 Characterization of the setup

After cool-down, the beat frequency initially exhibited a drift on the order of 1 Hz/s. After 2 months, this was reduced to 0.02 Hz/s. Our following discussion refers to this stable regime of operation.

A main characteristic of the apparatus, the frequency instability of the beat, is shown in Fig. 1.5. The root Allan variance (RAV) exhibits a peak at about 7 s. This is due to the modulation of the beat frequency by the pulse-tube cooler with peak-peak amplitude of about 400 Hz. Although the cooler has a mechanical frequency at 1.1 Hz, this frequency was aliased to a lower frequency by the 1 s sampling time of the frequency counter. The minimum RAV ($7 \cdot 10^{-15}$) is attained at $\tau = 20 - 30$ s. At the half-period of the rotation, 300 s, the RAV has increased to $1.4 \cdot 10^{-14}$. The main reasons for this level

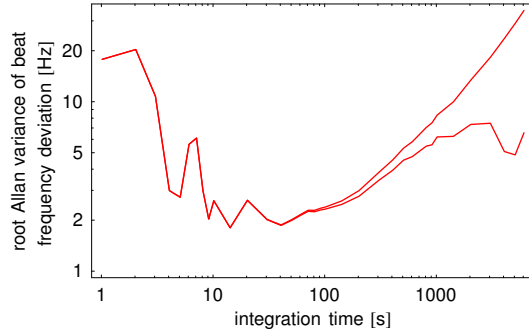


Fig. 1.5. Root Allan variance of beat frequency under rotation (without tilt correction and temperature decorrelation). Upper curve: from raw data including drift; lower curve: after removal of the drift (approx. 0.02 Hz/s) from raw data. The time record is the same as in Fig. 1.7, left.

appear to have been due to a low signal-to-noise ratio of the error signal and to the presence of mechanical/thermal noise from the cooler components and from the laboratory. These RAV values are about an order of magnitude higher than those obtained for the same integration time in the previous, nonrotating, experiment using these resonators [3]. However, for the purpose of the isotropy test the relevant integration time was $\tau = 12$ h in the latter experiment, for which the instability was higher than that at 300 s, relevant in the present experiment.

1.3.1 Laser power

The dependence of the TEM_{00} resonance frequencies on the power of the beam impinging on the resonators could reliably be measured only for relatively large power changes ($> 5 \mu\text{W}$) and was dependent on the mode-match efficiency. For the resonator with the larger sensitivity, a conservative upper limit is 50 Hz/ μW . For the power levels reaching the cavities and the relative power instability given above, this implies an influence of the residual power fluctuations of not more than 0.5 Hz ($1.8 \cdot 10^{-15}$).

1.3.2 Tilt of the resonators

The sensitivity of the beat frequency on the orientation of the cryostat was measured.

The experiment was operated on an optical table that was not floated but was supported by a metal frame. The lengths of the feet of the frame could be changed by acting on screws. Before each run, the tilt sensitivities were determined by measuring the frequency shift as function of the inclination of the cryostat in two orthogonal directions. To this end, the leg screws were

turned and the orientation of the optical table as a whole was changed. The resulting cryostat inclination was measured by a sensitive two-axis tilt-sensor attached to the plate that holds the cryostat. The resolution of the tilt sensor was $0.1 \mu\text{rad}$. The tilt sensor output showed a small dependence on the temperature, but this effect was suppressed by a passive temperature insulation.

We measured a sensitivity of about $0.06 \text{ Hz}/\mu\text{rad}$ for tilts around two axes parallel to the resonator axes. Typically, the peak-to-peak tilt variation during rotation was $80 \mu\text{rad}$, corresponding to 5 Hz beat modulation. Because of this magnitude, the tilt effects were taken into account in the data analysis.

1.3.3 Temperature sensitivities

We measured the dependence of the beat frequency on the temperature of the optical bench by changing the set-point of the temperature controller. The temperature was measured using a Cernox sensor (Lakeshore), connected to the housing of one of the two cavities. Because of the high thermal conductivity of the bench the temperature difference between the two resonators is expected to be very small. The temperature sensitivity was 1.5 Hz/mK . This is equivalent to a thermal expansion coefficient difference between the two cavities of $5.3 \cdot 10^{-12}/\text{K}$, a value 15 times lower than the nominal expansion coefficient of sapphire at the same temperature.

The typical residual temperature variation correlated with rotation are 0.15 mK peak-to-peak, leading to an influence on the beat frequency of 0.2 Hz ($0.8 \cdot 10^{-15}$). The instability of the temperature of the optical bench for various time scales is shown in Fig. 1.6.

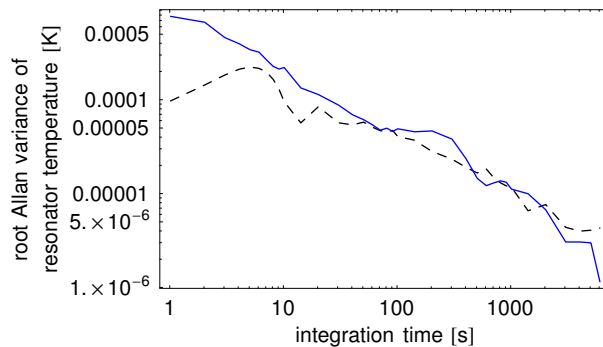


Fig. 1.6. Root Allan variance of the (actively stabilized) temperature measured near one of the resonators. Full line: with rotations: the plateau at 300 s is due to a (residual) modulation correlated with rotation. The time record is the same as in Fig. 1.7. Dashed line: from a record without rotations.

Ambient and cryostat component temperatures did have a significant effect on the beat frequency.

The sensitivity of the beat frequency to changes of the temperature in the lab was measured by acting on the air conditioning system. A sensitivity of approx. 75 Hz/K was measured. We did not observe any strong correlation between the lab temperature and the temperature of the optical bench cold plate. When the lab temperature was modulated so as to give 40 Hz beat modulation, the cold plate temperature's peak-peak amplitude was smaller than 0.3 mK, corresponding to a calculated beat frequency modulation of less than 0.5 Hz. Thus, it appears that the observed temperature sensitivity of the beat frequency was due to the thermal sensitivity of the fibers. Temperature changes affected their optical path length and in the presence of residual amplitude modulation and spurious etalons the laser frequency lock point changed. The fiber temperature is influenced both directly by the ambient temperature (detectable by heating the fibers locally) and by their contact to various parts of the cooler inside the cryostat, whose temperatures also changed with ambient temperature and cooler operating conditions.

Typical temperature variations measured at the top of the cryostat during one rotation were as low as 25 mK peak-peak after improvements in the temperature insulation of the setup, corresponding to a 2 Hz peak-to-peak effect assuming the above temperature sensitivity.

In order to characterize to what extent the various temperature variations induced beat frequency variations, we analyzed the correlations. The monitored temperatures were two laboratory temperatures measured at the top and bottom of the cryostat, four temperatures on different cooler components inside the cryostat and the temperature of one resonator holder. A linear regression analysis showed that there are strong correlations between these parameters and the beat frequency. Fig. 1.7 shows an example of this analysis. As can be seen, the slow variations of the beat frequency with respect to a nearly constant drift are to a large extent removed.

A summary of the systematic effects is given in Table 1.1. Not included are sensitivities to the temperatures of individual refrigerator components, since they could not be measured.

1.4 Data collection and analysis

A computer-controlled rotation stage rotated the cryostat over a range of 90°. The total range accessible was limited to a value slightly above this by the He pressure lines connecting the pulse-tube cooler with the stationary compressor. The period of rotation was chosen as 600 s. Shorter periods led to a significant shaking of the cryostat and were therefore not used.

Two synchronized computers collected the data. One computer controlled the rotation angle and rotation speed of the experiment, recorded the beat frequency and the temperature of the optical resonators, by means of a program

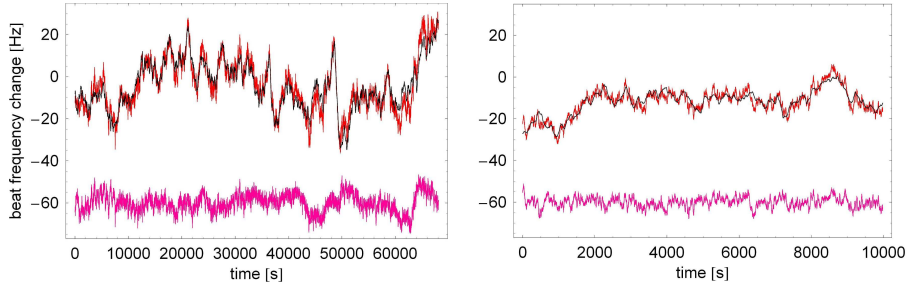


Fig. 1.7. Influence of temperature variations. Left: decorrelation of a 70 ks long beat frequency data set; right: decorrelation of a 10 ks subset starting at 50 ks. Red: beat frequency, after subtraction of linear and quadratic drift and correction for tilts. Black: Linear combination of seven temperature traces that best fits the corrected beat frequency. Pink (bottom traces): residuals, offset for clarity. During this measurement, the apparatus was rotated. Traces are averaged over 21 s.

written in LabView. Sampling time was 1 s. The second computer recorded the cryostat tilt angles, and several temperatures as mentioned above. The tilt and temperature values were used in the data analysis as explained below.

The data discussed here was obtained after about two years of testing and improvements on the whole system. Test runs performed initially typically exhibited significant drifts of properties of the apparatus, such as cooler internal temperatures. After minimizing these variations, we succeeded in obtaining stable operation.

For data analysis, the (aliased) beat frequency modulation was removed from the data by filtering in the Fourier domain, and the sum of the tilt angles multiplied by the respective tilt sensitivities was subtracted. Decorrelation of the temperatures was then performed, if desired.

The beat frequency in each interval $\theta = [0^\circ; 90^\circ; 0^\circ]$ (labeled by i) was least-squares fitted with the three-parameter function

Table 1.1. Characterized systematic effects. The column "Inst/mod" lists the measured parameter instability on the timescale of the rotation half-period or the peak-peak modulation. The column "Systematic" is the product of the first column and the sensitivity coefficient. The estimates of the systematics are indicative, since we do not distinguish between angular variations of type $\cos\theta$, $\sin\theta$ and $\cos 2\theta$, $\sin 2\theta$, the two latter types being the relevant ones for the isotropy test.

Effect	Inst/mod	Sensitivity	Systematic	Relative
Tilt	50 μrad	0.06 Hz/ μrad	3 Hz	$1.1 \cdot 10^{-14}$
Ambient temperature	0.025 K	75 Hz/K	2 Hz	$0.7 \cdot 10^{-14}$
Resonator temperature	150 μK	1.5 Hz/mK	0.2 Hz	$0.8 \cdot 10^{-15}$
Laser power	10 nW	50 Hz/ μW	0.5 Hz	$1.8 \cdot 10^{-15}$

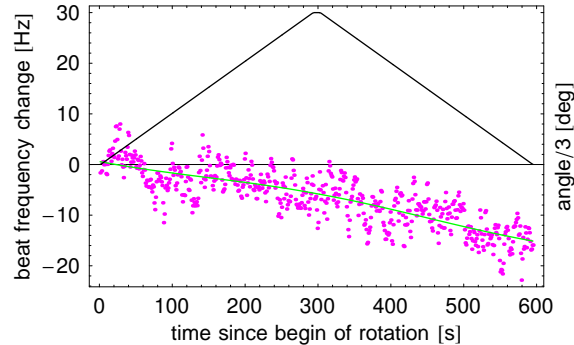


Fig. 1.8. Beat frequency as a function of rotation of the apparatus. Pink dots: tilt-corrected beat frequency, cooler-induced modulation removed, no averaging, 1s sampling time; green line: fit of beat frequency according to Eq.(1.2) with values $2C\nu = -0.76 \pm 0.18$ Hz, $2B\nu = -0.02 \pm 0.41$ Hz; black line: angular position.

$$a_i t + 2B(t_i) \sin 2\theta(t) + 2C(t_i) \cos 2\theta(t), \quad (1.2)$$

where the coefficient a_i quantifies a linear drift that may vary from rotation to rotation. An example of an analysis of a single rotation is shown in Fig. 1.8. The obtained amplitude sets $\{2B(t_i)\}$, $\{2C(t_i)\}$ are then analyzed according to the Robertson-Mansouri-Sexl test theory and the Standard Model Extension.

1.4.1 Analysis in the RMS framework

It can be shown [8] that according to the RMS test theory, the amplitudes of the beat frequency modulation with angle are given by

$$2B(t) = (1/2 - \beta + \delta)(v^2/c_0^2)(\gamma_3 \cos \omega_{\oplus} T_{\oplus} + \gamma_4 \cos 2\omega_{\oplus} T_{\oplus} + \sigma_3 \sin \omega_{\oplus} T_{\oplus} + \sigma_4 \sin 2\omega_{\oplus} T_{\oplus}), \quad (1.3)$$

$$2C(t) = (1/2 - \beta + \delta)(v^2/c_0^2)(\gamma_0 + \gamma_1 \cos \omega_{\oplus} T_{\oplus} + \gamma_2 \cos 2\omega_{\oplus} T_{\oplus} + \sigma_1 \sin \omega_{\oplus} T_{\oplus} + \sigma_2 \sin 2\omega_{\oplus} T_{\oplus}), \quad (1.4)$$

where the constants are defined in Table 1.2.

T_{\oplus} is the time since the beginning of the data plus an offset that accounts for a time difference since the coincidence of the lab's y axis with the \hat{Y} axis of the Sun-centered system [5]. The y axis is parallel to one cavity axis when in the 0° position. The direction of the Sun's velocity \mathbf{v} relative to the cosmic microwave background is given by the right ascension $\Phi = 168^\circ$ and the declination $\Theta = -6^\circ$.

In order to provide an analysis similar to that of [19, 20], we consider a measurement interval extending over 183 hours that contained 940 rotations (after removal of a small number of outliers), grouped in 5 sets. Only the tilt correction was implemented and each set was fitted with the functions (1.3) and (1.4) plus additional contributions $b_{syst} + b'_{syst}t_i$ and $c_{syst} + c'_{syst}t_i$ that model systematic effects. The individual sets yield the following values and standard errors for $\beta - \delta - 1/2$: $\{(5.5, 5.0), (7.2, 9.0), (-8.3, 3.7), (5.7, 4.5), (-2.6, 3.9)\} \cdot 10^{-10}$. The overall result is

$$\beta - \delta - 1/2 = (-0.6 \pm 2.1 \pm 1.2) \cdot 10^{-10} , \quad (1.5)$$

where the first error is statistical and the second error reflects the uncertainty in the experimentally determined tilt sensitivities and an estimate of the influence of laser power variations.

1.4.2 SME test theory

Considering that the time span over which data was taken was significantly less than one year, the main goal of the data analysis within the SME model was the determination of a value for $(\tilde{\kappa}_{e-})^{ZZ}$. The results of the cryogenic microwave experiment [4] found the elements of $(\tilde{\kappa}_{e-})$ (except for $(\tilde{\kappa}_{e-})^{ZZ}$) and the elements of $\beta_{\oplus}(\tilde{\kappa}_{o+})$ to be at most several parts in 10^{-15} in magnitude. If we assume these elements to be zero, we can use the result for $2C$ only to determine $(\tilde{\kappa}_{e-})^{ZZ}$,

$$(\tilde{\kappa}_{e-})^{ZZ} = \frac{4\langle 2C \rangle}{3 \sin^2 \chi} . \quad (1.6)$$

For the set of rotations under the most stable conditions (of 76 hours duration, also considered in [8]) the average is $\langle 2C\nu \rangle = -2.4$ Hz with a sample standard deviation of 1.9 Hz, and $\langle 2B\nu \rangle = 0.8$ Hz, with a sample standard deviation 2.6 Hz. In this analysis, the frequency data was also decorrelated with respect to the temperature data, whereby data intervals of 10 ks were decorrelated individually, in order to allow for changing environmental conditions. Without decorrelation of the temperatures the values are, in the same order, $(-3.3$ Hz, 2.3 Hz) and $(2.8$ Hz, 2.4 Hz) [8].

We used the large number of rotations performed under different experimental conditions to estimate the uncertainty in $2C$ due to (identifiable)

Table 1.2. The values of γ_i and σ_i appearing in Eqs.(1.3) and (1.4).

$\gamma_0 = \frac{1}{4} \sin^2 \chi (3 \cos^2 \Theta - 1)$	
$\gamma_1 = \frac{1}{2} \cos \Phi \sin 2\Theta \sin 2\chi$	$\sigma_1 = \gamma_1 \tan \Phi$
$\gamma_2 = \frac{1}{4} \cos 2\Phi \cos^2 \Theta (\cos 2\chi - 3)$	$\sigma_2 = \gamma_2 \tan 2\Phi$
$\gamma_3 = \sigma_3 \tan \Phi$	$\sigma_3 = \cos \Phi \sin \chi \sin 2\Theta$
$\gamma_4 = -\sigma_4 \tan 2\Phi$	$\sigma_4 = \cos^2 \Theta \cos \chi \cos 2\Phi$

systematic effects at 1.8 Hz. This includes the errors due to the uncertainty of the tilt coefficients and due to laser power variations. This results in¹

$$(\tilde{\kappa}_{e-})^{ZZ} = (-2.9 \pm 2.2) \cdot 10^{-14} \quad , \quad (1.7)$$

where the uncertainty is dominated by the systematic effects.

1.5 Conclusions

The experiment described in this work was performed in order to improve the previous rotating laser experiment by Brilliet and Hall, exploiting some of advances in laser stabilization techniques developed since. Our experiment yielded a significant improvement. Similar to their experiment, a strong limit for $\beta - \delta - 1/2$ required exploiting the modulation by Earth's rotation. At the same time the present experiment provided an approach to the task of measuring $(\tilde{\kappa}_{e-})^{ZZ}$ with high accuracy (a weaker limit on this quantity can also be extracted from the experiment of Brilliet and Hall).

Limitations of the experiment were the sensitivity of the optical path length to temperature, and the limited laser lock quality as a consequence of the relatively weak cavity throughput. This made the beat frequency more sensitive to optical path length variations. In addition, a certain level of mechanical noise was present. In an upgraded experiment, obvious improvements are resonators of higher finesse and throughput, optical path length stabilization, and rotations with shorter period and lower tilt modulation.

In discussing a "null" experiment, it may be argued that a nonzero value of the measured parameter may have been (partially) canceled by an unknown systematic effect, so that the bounds provided by an experiment may be questioned. We emphasize the importance of the fact that three experiments [8, 19, 20] have recently been reported whose results are consistent with each other. Because they were performed by independent groups with different techniques, it is unlikely that they all exhibit a strong cancellation between the respective systematics and a substantial nonzero value of $(\tilde{\kappa}_{e-})^{ZZ}$.

Acknowledgments We thank E. Göklü for his participation in this work, L. Haiberger for contributions to the cryostat development, A. Nevsky and C. Lämmerzahl for discussions, and G. Thummes for his helpful assistance. P.A. was supported by a DAAD fellowship, M.O. by a Heinrich-Hertz Foundation fellowship. This research was part of the Gerhard-Hess Program of the German Science Foundation.

References

1. Brilliet, A. and Hall, J. *Phys. Rev. Lett.* **42**, 549 (1979).

¹In [8], a factor 2 was inadvertently omitted when calculating $(\tilde{\kappa}_{e-})^{ZZ}$ from $2C$.

2. Lipa, J. A., Nissen, J. A., Wang, S., Stricker, D. A., and Avaloff, D. *Phys. Rev. Lett.* **90**, 060403 (2003).
3. Müller, H., Herrmann, S., Braxmaier, C., Schiller, S., and Peters, A. *Phys. Rev. Lett.* **91**, 020401 (2003).
4. Wolf, P., Bize, S., Clairon, A., Santarelli, G., Tobar, M. E., and Luiten, A. N. *Phys. Rev. D* **70**, 051902(R) (2004).
5. Kostelecký, V. and Mewes, M. *Phys. Rev. D* **66**, 056005 (2002).
6. Kostelecký, V. and Mewes, M. *Phys. Rev. Lett.* **87**, 251304 (2001).
7. Mansouri, R. and Sexl, R. *Gen. Rel. and Grav.* **8**, 497 (1977).
8. Antonini, P., Okhapkin, M., Göklü, E., and Schiller, S. *Phys. Rev. A* **71**, 050101(R) (2005).
9. Braxmaier, C., Müller, H., Pradl, O., Mlynek, J., Peters, A., and Schiller, S. *Phys. Rev. Lett.* **88**, 010401 (2002).
10. Wang, C. and *et al.* *Cryogenics* **37**, 159 (1997).
11. Lienherth, C. and *et al.* *IEEE Trans. on Applied Superconductivity* **11**, 812 (2001).
12. Seel, S., Storz, R., Ruoso, G., Mlynek, J., and Schiller, S. *Phys. Rev. Lett.* **78**, 4741 (1997).
13. Storz, R., Braxmaier, C., Jäck, K., Pradl, O., and Schiller, S. *Opt. Lett.* **23**, 1031 (1998).
14. Müller, H., Braxmaier, C., Hermann, S., Pradl, O., Lämmerzahl, C., Mlynek, J., Schiller, S., and Peters, A. *IJMPD* **11**, 1101 (2002).
15. Lucht, M., Lerche, M., Wille, H. C., Shvyd'ko, Y. V., Rüter, H. D., Gerdau, E., and Becker, P. *J. Appl. Cryst.* **36**, 1075 (2003).
16. Storz, R. Phd thesis, Universität Konstanz, Germany, (1998).
17. Drever, R. W. P., Hall, J. L., Kowalski, F. V., Hough, J., Ford, G. M., Munley, A. J., and Ward, H. *Appl. Phys. B* **31**, 97 (1983).
18. Cantatore, G., Valle, F. D., Milotti, E., Pace, P., Zavattini, E., Polacco, E., Perrone, F., Rizzo, C., Zavattini, G., and Ruoso, G. *Rev. Sci. Instrum.* **66**, 2785 (1994).
19. Stanwix, P. L., Tobar, M. E., Wolf, P., Susli, M., Locke, C. R., Ivanov, E. N., Winterflood, J., and van Kann, F. *Phys. Rev. Lett.* **95**, 040404 (2005).
20. Herrmann, S., Senger, A., Kovalchuk, E., Müller, H., and Peters, A. *arXiv physics*, 0508097 (2005).